

**Evidence of boundary reflection of Kelvin and first-mode Rossby waves
from TOPEX/POSEIDON sea level data**

Jean-Philippe Boulanger* and Lee-Lucng Fu

Jet Propulsion Laboratory

Ms 300-323

4800 Oak Grove Drive

Pasadena, CA 91109

*E-mail: jpb@pacific.jpl.nasa.gov

Submitted to *Journal of Geophysical Research-oceans*

Submitted November 1995

Revised March 1996

Abstract

The TOPEX/POSEIDON sea level data leads to new opportunities to investigate some theoretical mechanisms suggested to be involved in the El Niño/Southern Oscillation phenomenon in the tropical Pacific ocean. In particular, we are interested in studying the western boundary reflection, a process crucial for the delayed action oscillator theory, by using the TOPEX/POSEIDON data from November 1992 to May 1995. We first projected the sea level data onto Kelvin and first-mode Rossby waves. Then we estimated the contribution of wind forcing to these waves by using a single **baroclinic** mode simple wave model forced by the ERS-1 wind data. Wave propagation was clearly observed with amplitudes well explained by the wind forcing in the ocean interior. Evidence of wave reflection was detected at both the western and eastern boundaries of the tropical Pacific ocean. At the eastern boundary, Kelvin waves were seen to reflect as first-mode Rossby waves during the entire period. The reflection efficiency (in terms of wave amplitude) of the South-America coasts was estimated to be 80% of that of an infinite meridional wall. At the western boundary, reflection was observed in April-August 1993, in January-June 1994 and, later, in December 1994-March 1995. Although the general roles of these reflection events in the variability observed in the equatorial Pacific ocean are not clear, the data suggest that the reflection in January-June 1994 have played a role in the onset of the warm conditions observed in late 1994-early 1995. Indeed, during the January-June 1994 period, as strong **downwelling** first-mode Rossby waves reflected into downwelling Kelvin waves, easterly wind and cold sea surface temperature anomalies located near the date line weakened and eventually reversed in June-July 1994. The presence of the warm anomalies near the date line then favored convection and westerly wind anomalies that triggered strong **downwelling** Kelvin waves propagating throughout the basin simultaneously with the beginning of the 1994-1995 warm conditions.

1. Introduction

The delayed action oscillator has been suggested by Schopf and Suarez (1988) to be a potential mechanism for the El Niño/Southern Oscillation (ENSO). Battisti (1988) described this theory in the light of long equatorial wave propagation and reflection. The essence of the theory can be summarized as follows: considering an initial warm anomaly in the central Pacific, the atmosphere first responds by westerly wind anomalies west of the initial warm anomaly. The wind anomalies then force eastward-propagating **downwelling** Kelvin waves which favor the growth of the anomaly and **upwelling** long Rossby waves which propagate towards the western Pacific where they **reflect** into **upwelling** Kelvin waves. These waves travel back to the region of the unstable anomaly, where they act against its growth until they cancel and eventually reverse it into a cold anomaly which, in turn, grows subsequently. Related to the growth of this cold anomaly, easterly wind anomalies take place in the central Pacific and force eastward-propagating **upwelling** Kelvin waves which favor the growth of the cold anomaly and westward-propagating **downwelling** Rossby waves. The same scenario as described above for the warm anomaly (but of opposite sign) is then at work to reverse **the** cold anomaly eventually. ENSO-like oscillations are thus periodic, and the period depends on the long wave propagation and reflection and on local coupled unstable **processes** in the central Pacific. In the case of a warm event, the time delay between the first **upwelling** Kelvin wave generated by Rossby wave reflection and the reversal of the warm anomaly in the central Pacific is around 18 months.

To investigate various potential ENSO mechanisms, Li and Clarke (1994) studied historical data of sea level at the eastern and the western boundaries of the Pacific together with zonally averaged equatorial wind. They concluded that the buildup theory described by Wyrtki (1975) was consistent with their results. They suggested Rossby wave reflection at **the** western boundary to contribute to the ocean and atmosphere dynamics in the Pacific interior. But they did not find the Kelvin wave signal in the western Pacific leading the reversal of the winds in the central Pacific by 18 months as stated by the delayed action oscillator mechanism **described** by Battisti (1988). Therefore they concluded that “extra physics beyond delayed action oscillator is necessary to

describe ENSO". To explain Li and Clarke (1994)'s results, **Mantua and Battisti** (1994) first showed that even if the delayed action oscillator were at work in the Pacific, the 18-month lag between the Kelvin signal in the western Pacific and the reversal of the winds in the central Pacific would not be found by Li and Clarke (1994)'s statistical analysis because of the aperiodic nature of ENSO. Therefore, they concluded that Li and Clarke (1994)'s results were not inconsistent with the **delayed** action oscillator theory, but that the scenario originally described by **Battisti** (1988) needed to be revisited. Thus **Mantua and Battisti** (1994) argued that, although this mechanism could not explain the lack of regularity of ENSO events, it provided a potential explanation for the growth and **decay** of these events. Therefore the western boundary reflection acts mainly as a termination mechanism for **the** warm events.

The previous results were based on the analysis and comparison of historical sea level data in the western Pacific and reduced-gravity shallow-water ocean model **hindcasts**. Now, synoptic observations of the Pacific provided by the TOGA-TAO (Tropical Ocean Global Atmosphere-Tropical **Atmosphere** Ocean; Hayes et al, 1991; McPhaden, 1993) mooring array and by satellites (such as **altimetric** data by GEOSAT from 1985 to 1989, by TOPEX/POSEIDON since **october** 1992, by ERS-1 since the end of 1991) can help us to investigate the validity of theoretical mechanisms for the basin-wide ocean-atmosphere system variability. After the detection of long equatorial wave propagation in **GEOSAT** data by **Delcroix et al.** (1991), **duPenhoat et al.** (1992) studied potential wave reflection at the eastern boundary by using a simple ocean model. Later, **Delcroix et al.** (1994) projected **GEOSAT** sea level and corresponding **geostrophic zonal** currents onto long equatorial waves over the 160°E-90°W region. They showed clear propagation of **Kelvin** and first-mode Rossby waves as **well** as their important contribution to the equatorial ocean dynamics during the 1986-1987 El Niño and 1988-1989 La Niña events. However, they did not **observe** any Rossby wave reflection contributing to the Kelvin wave amplitude in the central Pacific. Rather, wind forcing in the western Pacific appeared as a main trigger of Kelvin waves propagating towards the central and east Pacific. Investigating the displacement of the eastern edge of the Pacific warm-pool during the 1986-1989 ENSO period, **Picaut and Delcroix** (1995) found that a strong **downwelling** first-mode Rossby wave (partly reflected at the **eastern** boundary from a **downwelling**

Kelvin wave and partly wind forced along its path) induced strong westward geostrophic zonal currents at the end of 1987. They further argued that this wave could have pushed back the eastern edge of the warm pool and have been responsible for the switch from the 1986-1987 El Niño to the 1988-1989 La Niña. Such a scenario disagrees with the delayed action oscillator theory. Using mainly the TOGA-TAO buoy array data, Kessler and McPhaden (1995) investigated the equatorial dynamics over the 1991-1993 ENSO period. They advocated that the reflection of an upwelling Rossby wave at the western boundary terminated the 1991-1992 El Niño event, but they did not observe any downwelling Rossby wave as a precursor for the 1992-1993 warm event. They concluded that the propagation and reflection of equatorial waves cannot fully explain the occurrence of ENSO event. Their result seems consistent with Mantua and Battisti (1994)'s conclusion: the delayed action oscillator may explain the termination of the warm events, but a coupled mechanism responsible for the initial unstable perturbation is beyond this theory.

Recently, Boulanger and Menkes (1995) presented a method to calculate long equatorial wave coefficients from sea level data throughout the equatorial Pacific basin. They applied it to TOGA-TAO dynamic height and TOPEX sea level data during the November 1992-December 1993 period. Having found evidence for the propagation of Kelvin and first to third mode Rossby waves at theoretical phase speeds, they investigated the reflection of long waves at both boundaries. They did not observe any clear reflection at either boundary and concluded that, during the period under study, wind forcing was a major trigger of Kelvin and first Rossby waves propagating in the central Pacific.

The previous studies highlighted the missing initial perturbation mechanism for ENSO events and gave different explanations for the termination of the 1986-1987 and 1991-1992 warm ENSO events. Although the short period of TOPEX/POSEIDON sea level data does not allow the study of the role of reflection in the interannual variability as done by Mantua and Battisti (1994), we can investigate the existence of long wave reflection at both boundaries of the Pacific ocean. In the present study, we use a different version of the TOPEX/POSEIDON data from that used by Boulanger and Menkes (1995). The results in terms of long wave coefficients are compared to a simple wind-driven model simulation to study potential boundary reflection of Kelvin and first-mode Rossby waves. This paper is organized as follows: Section 2 presents TOPEX/POSEIDON sea level

data processing as well as ERS-1 wind data over the November 1992-May 1995 period, the decomposition method of Boulanger and Menkes (1995) and the simple wind-driven model are briefly presented; Section 3 describes long wave propagation and their variability; Section 4 discusses long wave reflection at both the eastern and western boundaries; Section 5 suggests a potential role of the reflection observed in January-June 1994 in the onset of the warm conditions in late 1994-early 1995; finally, Section 6 presents conclusions.

IL Data and analysis methods

The TOPEX/POSEIDON sea level data (Fu et al., 1994) from October 1992 to June 1995 were used in the study. Standard instrument and environmental corrections (including the inverted barometer effect) were applied (Callahan, 1994). Additionally, the tide model of Ma et al. (1994) based on the TOPEX/POSEIDON data was also applied. Along-track data were binned every cycle into a 3° longitude by 0.5° latitude grid for the analysis discussed below. There are two differences from the data described by Menkes et al. (1995) and used by Boulanger and Menkes (1995). First, they used the tide model of Ray et al. (1994). Second, they binned along-track data into 10° longitude by 0.5° latitude boxes every 5° longitude. These differences may be responsible for the different results from the two studies especially near the ocean boundaries where high resolution is desired.

As we examine long wave propagation and reflection, we are interested in the low-frequency large-scale signal of the TOPEX/POSEIDON (T/P hereafter) sea level data. Therefore, the data are interpolated onto a 10-day time step and filtered with a 50-day Hanning filter (except specified otherwise). The method of Boulanger and Menkes (1995) was then used to project the sea level data, denoted $h(x,y,t)$ into the modes of long equatorial wave as follows:

$$h(x,y,t) = \sum_0^N r_n(x,t) R_n^h(y) \quad (1)$$

where r_n are the coefficients to be calculated by the method and $R_n(y)$ are long wave sea level structures (Figure 1; $n=0$ refers to Kelvin wave, n greater than 0 refers to the corresponding long Rossby wave). The sum is assumed to be finite ($N=20$; see Boulanger and Menkes (1995) for a discussion on the value of N). Only r_0 and r_1 are analyzed in the following.

We first construct sea level anomalies from the Kelvin and first-mode Rossby coefficients for comparison to the original T/P sea level data. Anomalies are computed relative to the mean of the January 1993-December 1994 period. Standard deviation of both the original and the reconstructed fields, the correlation between the two and the variance explained by the reconstructed field are displayed between 5°N and 5°S in Figures 2a-d. Poleward of these latitudes, the Kelvin and first-mode Rossby sea level amplitudes decrease exponentially. Correlation coefficients are higher than 0.8 over the entire 5°N-5°S region, and higher than 0.9 along the Equator. The agreement is poorer between 160°E and the date line where a minimum of sea level variability is observed. The sea level variance explained by the Kelvin and first-mode Rossby wave signals is higher than 80% in the 3°N-3°S band. The previous figures clearly show that these two equatorial waves explain most of the sea level variability in the equatorial band as already shown by similar comparisons made by Delcroix et al. (1994) and Boulanger and Menkes (1995).

To detect potential reflection of Kelvin and first-mode Rossby waves at either boundary, we need to estimate the wind forcing contribution to these wave signals. We used the ERS-1 zonal wind stress data provided by the "Centre ERS d'Archivage et de Traitement" located in the "Institut Français de Recherche pour l'Exploitation de la Mer". Data were first converted to wind stress using bulk formulae (Smith, 1988) and then gridded on a 10 longitude by 10 latitude grid every 7 days. At last, we interpolated the wind stress data onto a 10-day time step (as T/P sea level data) and filtered the data with a 50-day Hanning filter. We used the method described by Boulanger and Menkes (1995) to calculate the Kelvin and first-mode Rossby forcing coefficients. The following simple wave equations are then used to estimate the simulated wind-forced Kelvin and first-mode Rossby wave coefficients (denoted by s_0 and s_1):

$$(\partial_t + r_{\text{fric}} + c_0 \partial_x) s_0 = b_0 / (\rho_0 H) \quad (2)$$

$$(\partial_t + r_{\text{fric}} - \frac{c_0}{3} \partial_x) s_1 = b_1 / (\rho_0 H) \quad (3)$$

where b_0 and b_1 respectively denote the Kelvin and first-mode Rossby forcing coefficients, r_{fric} is a Rayleigh friction coefficient (chosen to correspond to a 3-month time scale; this value is consistent with the results of Picaut et al.(1993) and a similar study by Kessler and McPhaden (1995)), c_0 is the wave speed of the first baroclinic mode (2.5 m/s for a typical stratification in the tropical Pacific), H is the thickness of the shallow-water layer (80m), and ρ_0 is the density of sea water. This choice of parameters gives a good comparison to data. Our purpose is not to do a quantitative comparison between the long wave coefficients and our simple wave model. but rather to identify the periods and regions of major contributions of wind forcing to the observed long wave variability.

11.1. Long equatorial wave coefficients

Kelvin wave coefficient. Figures 3a and 3b respectively display the Kelvin wave coefficients derived from the T/P data and the wind-driven model simulation. A comparison of these two figures shows that most of the variability east of 160°E is well reproduced by the simple model. From November 1992 to May 1995, the Kelvin wave variability was mainly characterized by the following features. In boreal winter 1992-1993, westerly wind anomalies triggered downwelling Kelvin waves which propagated through the equatorial Pacific basin and reached the eastern boundary in the beginning of 1993. Later, during Spring 1993, westerly wind anomalies in the central and eastern Pacific forced more downwelling Kelvin waves. The following months of 1993 were then characterized by strong upwelling Kelvin waves and weak downwelling waves. While a strong upwelling Kelvin wave was observed in February-March 1994 east of the dateline, the signal from July 1994 to January 1995 was dominated by strong downwelling Kelvin waves related to the 1994-1995 warm event in the equatorial Pacific ocean. This short warm event terminated as upwelling Kelvin signals were observed throughout the basin in February and March 1995.

First, it is important to note that the variability observed in the Kelvin wave coefficient is very different from one year to another, leading to the conclusion that no evident seasonal cycle is apparent in the Kelvin wave variability over these two and a half years of data. Then, the comparison between Figures 3a and 3b shows that major differences are observed near the western boundary where the simulated Kelvin wave amplitude is much weaker than the amplitude of the T/P Kelvin wave. It is interesting to note that, when this missing signal was imposed as a boundary condition to the wind-forced model simulation, the resulting simulated amplitude became closer to the observed one. Therefore, most of the discrepancies between the model and T/P data in the central and east Pacific can be traced to the discrepancies in the western Pacific in terms of Kelvin waves. Whether this missing amplitude can be explained by first-mode Rossby wave reflection is an issue addressed later in the paper.

First-mode Rossby wave coefficient. Though differences between 1993, 1994 and the beginning of 1995 can be observed in Figures 4a and 4b, the first-mode Rossby coefficients appears to be dominated by a seasonal cycle. This seasonal cycle can be described as follows. In January, as the Trades along the equator are strong, downwelling Rossby waves are forced near 140°W. During spring, as the Trades weaken, upwelling Rossby waves are generated in the east Pacific. Then later, as the ITCZ is moving northward and the Trades strengthen, other downwelling first-mode Rossby waves are triggered in the east Pacific. This signal decreases in the eastern Pacific until January when a downwelling Rossby wave is then forced.

Main differences between 1993, 1994 and the beginning of 1995 are observed near the boundaries. On the two left panels of Figure 5, the Kelvin wave coefficients and the first-mode Rossby wave coefficients (reversed from east to west) display a strong correlation at the eastern boundary. As observed in Figure 5b, the upwelling Rossby wave signal in spring was found closer to the eastern boundary in 1994 than in 1993. This can be explained as follows. Downwelling Kelvin waves were impinging at the eastern boundary from December 1992 to June 1993, while strong upwelling Kelvin waves were observed east of the date line from January to April 1994. The reflection of the 1993 downwelling Kelvin waves certainly cancelled part of the 1993 upwelling

Rossby wave; the reflection of the 1994 upwelling Kelvin waves strengthened the 1994 upwelling Rossby wave.

Moreover, the downwelling Rossby wave initiated in summer is found coming from the eastern boundary in 1993, not in 1994. This is because, strong downwelling Kelvin waves were impinging at the eastern boundary in spring/summer 1993, but not in 1994. Similarly impinging downwelling Kelvin waves in November-December 1994 seemed to be responsible for the strong downwelling Rossby signal observed near the boundary. As this signal propagated westward, it was interfered by the wind-forced upwelling signal (Fig. 4b). This interference explained the differences in amplitude between the simulated and observed upwelling Rossby waves in Spring 1995 west of 110°W.

Therefore, the reflection of Kelvin waves explains the differences between the observation and the model simulation near the eastern boundary, and it also explains the differences in the observed Rossby wave signal in this region between 1993, 1994 and beginning of 1995. Near the western boundary, the main differences between 1993 and 1994 were observed during January-June 1994 when strong downwelling Rossby signals were observed west of the date line. At this time, downwelling Kelvin waves (Fig. 5C), not fully explained by the wind variability (Fig. 3b), were found in the western Pacific, indicating potential wave reflection of the downwelling Rossby waves at the western boundary. We now examine in more details the Kelvin and first-mode Rossby wave coefficients near the boundaries.

IV. Long equatorial wave reflection

Eastern boundary reflection. We first look at two longitudes 84°W and 93°W which are respectively located east and west of the Galapagos islands. If reflection occurs near 80°W at the coast of South America, the phase lag between the Kelvin and first-mode Rossby wave coefficients at the two longitudes are respectively 10 and 30 days (for a 2.5m/s Kelvin wave phase speed). Figure 6a displays the Kelvin coefficient with a 10-day lag (dashed line) and the first-mode Rossby

coefficient (solid line). The correlation between the two is 0.85, whereas the correlation between the Kelvin coefficient without the 10-day lag (not shown) and the first-mode Rossby coefficients is only 0.78. The Kelvin and first-mode Rossby coefficients have similar amplitudes. Therefore, it seems that during most of the period, the Kelvin and first-mode Rossby signals are correlated and their ratio of amplitudes is close to one. In theory, if the South America coast were an infinite wall, the reflection coefficient would be equal to 1.2 (Boulangier and Menkes, 1995). Therefore, our study leads to an 80% reflection efficiency of the eastern boundary.

A similar comparison was made west of the Galapagos Islands to examine if long wave amplitudes are affected along their propagation. Figure 6b displays the Kelvin coefficient with a 30-day lag (dashed line) and the first-mode Rossby coefficient (solid line) at 93°W. The correlation between the two is 0.81, whereas the correlation between the Kelvin coefficient with no lag and the first-mode Rossby coefficient is only 0.64. This result confirms the relationship between the Kelvin and first-mode Rossby waves due to the reflection occurring at the eastern Pacific boundary. However, the ratio of the first-Rossby wave coefficient to the Kelvin wave coefficient is dropped to 0.8. Kelvin wave coefficients at the two longitudes (Figure 6c) are correlated at 0.90 and their ratio of amplitudes is close to 1. However, Rossby wave coefficients (Figure 6d) are correlated at 0.81, and their ratio of amplitudes is equal to 0.8.

It is not clear why the Galapagos Islands would affect the first-mode Rossby wave and not the Kelvin wave. However, it seems plausible that this decrease in the Rossby wave amplitude would be due to the vertical energy propagation described by Kessler and McCreary (1993). In their study, they described the first-mode Rossby wave as the sum of many of its vertical modes (fifty in their study). The higher vertical modes have slower vertical propagation and thus are more likely to lose their energy. When projecting sea level onto the structures of the first baroclinic mode, leakage of energy from the high modes is inevitable. Therefore, a vertical energy propagation might be manifested in our Rossby coefficient by a decrease of its amplitude along the propagation. The use of a strong Rayleigh friction coefficient (3-month time scale) in the simple model is then a crude way to simulate the vertical propagation of energy in our one-layer model.

Western boundary rejection. As mentioned in **Boulangier** and Menkes (1995), the wave coefficient calculation is valid only when the southern boundary of the data is southward of 2°S . Therefore, we study reflection at the western boundary by investigating potential relationship between the Kelvin and first-mode Rossby wave coefficients at 144°E instead of locations further west where the southern boundary is north of 2°S . Due to a possible bias by tides at 60-day period (aliased M2 period in T/P data) in the western Pacific region, we decided to filter the sea level data by a 90-day Hanning filter. The time for a first-mode Rossby wave to travel from 144°E to the western boundary (130°E), to reflect and travel back to 144°E as a Kelvin wave is around 30 days. Thus, Figure 7a displays the Kelvin coefficient and the first-mode Rossby wave coefficient with a 30-day lag at 144°E . The correlation between the two is 0.54, whereas the correlation between the Kelvin coefficient and the first-mode Rossby coefficient with no lag is 0.24.

If a Rossby wave of amplitude of unity is to reflect at the western boundary, the amplitude of the Kelvin wave will be 0.41 (**Boulangier** and Menkes, 1995). In Figure 7a, the difference between the Kelvin wave amplitude and the Rossby wave amplitude multiplied by 0.41 is plotted. This time series represents the signal unexplained by the reflection. For the sake of comparison, this time series is also plotted in Figure 7b together with the simulated Kelvin wave amplitude at 144°E . It appears that the wind-forced Kelvin amplitude is rather weak compared to the signal not explained by the reflection. Finally, from Figures 7a-b, it appears that the reflection of Rossby waves into Kelvin waves is fairly well demonstrated from April to August 1993, from January to June 1994 and from December to February 1995. It is worth noting that the reflection of **upwelling** Rossby waves in 1993 occurred while the 1992-1993 El Niño conditions were weakening, that the reflection of **downwelling** Rossby waves in January-June 1994 occurred prior to the onset of the 1994-1995 warm conditions in the central and eastern Pacific, and, finally, that the reflection of **upwelling** Rossby waves (clearly observed in January-February 1995) occurred prior to the end of this short warm event.

Investigating the **actual** role of the reflection of first-mode Rossby waves in the termination of the 1992-1993 and 1994-1995 warm events and in the onset of the 1994-1995 warm event is beyond the scope of the present paper. However, we will show in the next section that the data suggest a **possible** role of the reflection in January-July 1994 in the onset of the warm conditions observed in

the equatorial Pacific in late 1994-early 1995. Finally, while reflection at the western boundary is unambiguously observed in the data, it is **puzzling** that reflection is observed only intermittently during the period of study. This raises crucial questions such as: **Is** reflection of the first-mode Rossby wave **occurring** all the time but is hidden by other processes contributing to the Kelvin wave signal? What other processes can efficiently contribute to the equatorial Kelvin wave amplitude? These questions are worth of investigation in the future.

V. The reflection in 1994 and the onset of the warm conditions in early 1994-late 1995

As noted above, the reflection of the Rossby waves at the western boundary in early 1994 seems to be related to the subsequent warm conditions observed in the Pacific ocean in late 1994. From November 1993 to February 1994, the eastern edge of the warm-pool (SST higher than 28°C) was displaced westward (Figure 8a) **while** a **downwelling** first-mode Rossby wave was observed in **the** central Pacific (Figure 4a). Related to this **displacement**, strong cold SST anomalies (more than -1.0°C) were observed from 170°E to 150°W (Figure 8b). On the west side of these anomalies, easterly wind anomalies in early 1994 (Figure 8c) were generating strong eastward propagating **upwelling** Kelvin and westward propagating **downwelling** Rossby waves. The latter **reflected** into **downwelling** Kelvin waves which could not reach the eastern Pacific ocean due to the easterly anomalies near the date line. However, they **cancelled** part of the wind-forced signal and **acted** against **the** negative SST anomalies, which indeed decreased in April-May near the date line. When these anomalies were **cancelled** and eventually switched to positive SST anomalies in July 1994 (SST was then higher than 30°C at the date line), a strong **downwelling** Kelvin wave (not fully explained by the local wind-forcing) propagated to the central Pacific ocean (Fig. 3a). Following the reversal of the wind and SST anomalies in the central Pacific, strong **downwelling** Kelvin waves were forced during late 1994-early 1995. Warm conditions were then observed in **the** equatorial Pacific ocean. Therefore, the conditions observed during the January-July 1994 period lead to the possibility that the reflection of **downwelling** Rossby waves into **downwelling** Kelvin waves may have played the role of an onset mechanism for the late 1994 warm conditions.

VI. Summary and conclusions

Following **Boullanger and Menkes (1995)**'s decomposition method, the **TOPEX/POSEIDON** sea level data are projected onto long equatorial wave structures. In this study, we only focus on Kelvin and first-mode Rossby waves. The sea level variance explained by these two waves is higher than 80% over the **3°N-3°S** equatorial band with maxima close to 96% at the equator. Lower values are found west of the date line from **160°E** to 180°. Clear propagation of Kelvin and first-mode **Rossby** waves is observed during the entire period. The Kelvin wave coefficient displayed a strong variability γ from 1993, 1994 and the beginning of 1995. No seasonal cycle is apparent in the Kelvin wave signal during the two and half years that this study covers. While **downwelling** Kelvin waves were observed in the central and eastern Pacific ocean in **early** 1993, the signal in early 1994 is mainly **upwelling**. West of the date line, **downwelling** signal is observed in most of 1994 while **upwelling** signal is observed in 1993. A much stronger **downwelling** signal is observed in late 1994 east of the date line simultaneously with the warming observed in the Pacific ocean. In the beginning of 1995, the termination of this short warm event is concomitant with the presence of **upwelling** Kelvin waves throughout the basin.

The Rossby signal is primarily dominated by an annual cycle. **Downwelling** waves are generated west of 110°W during **December-January**, followed by the annual **upwelling** Rossby wave related to the weakening of the Trades in spring. Subsequently, **downwelling** Rossby waves are observed again in July in the eastern Pacific. However, differences can be observed between 1993, 1994 and the beginning of 1995. **These** differences mainly appear near the boundaries. At the eastern boundary, the Rossby signal is generally correlated with the impinging Kelvin signal consistent with the wave reflection theory. At the western boundary, the differences in the Rossby signal are found to be related to the wind forcing located near the date line. Occasional evidence is found for the reflection of Rossby waves into Kelvin waves.

In the present study, we **found** that eastern boundary reflection indeed **occured** during the November 1992-May 1995 period and affected the **Rossby** wave amplitude at least to 140°W. The

reflection efficiency of the South America coasts (in terms of wave amplitude) was estimated to be 80% of that of an infinite meridional wall. No main differences were observed between Kelvin signal east and west of the Galapagos Islands, leading to the conclusion that these islands do not affect Kelvin waves in their propagation or amplitude. However, the Rossby wave amplitudes are decreasing while propagating from the coast to west of the Islands. This feature can be explained by the vertical energy propagation of Rossby waves (Kessler and McCrory, 1993). Although the delayed action oscillator mechanism does not give a role to the eastern boundary reflection in the interannual variability (Battisti, 1988), the strong evidence of this reflection during the entire period of study calls for future investigation of its actual role in the tropical Pacific ocean-atmosphere coupled variability.

At the western boundary, reflection of first-mode Rossby waves is observed in April-August 1993, in January-June 1994 and in December 1994-February 1995. These three events occurred respectively prior to the termination of the 1992-1993 El Niño, to the onset of the short warm 1994-1995 event and to its termination. Whether the reflection played a role in the equatorial Pacific ocean-atmosphere coupled system, as suggested by the delayed action oscillator, is not rigorously investigated in the present paper. However, the data do suggest a possible role of the reflection in the onset of the warm conditions. Indeed, while reflection occurred in January-June 1994, easterly wind and cold sea surface temperature anomalies located near the date line weakened. Potentially due to the action of reflected downwelling Kelvin waves, these anomalies eventually reversed in June-July 1994 into westerly wind and warm sea surface temperature anomalies. The growth of warm conditions near the date line subsequently generated a series of strong downwelling Kelvin waves propagating to the eastern Pacific simultaneously with the 1994-1995 warming in the Pacific ocean. The actual role of these reflected waves on sea surface temperature in the central Pacific will have to be investigated.

An important point we want to strengthen is that, except during the three periods when reflection is demonstrated, the Kelvin wave amplitude in the western Pacific is neither explained by reflection, nor by the wind forcing. It then leads to crucial questions such as to determine whether reflection occurs all the time but is hidden by other processes. As examples, potential sources for the

equatorial Kelvin wave amplitude could be the reflection of higher mode Rossby waves or coastal Kelvin waves propagating **equatorward** along the Papua/New Guinea coasts.

Finally, even if the delayed action oscillator theory gains some support from the existence of western boundary reflection, it is not yet demonstrated that reflection played the role suggested by this theoretical mechanism. Moreover, the short period under study (two and a half years) has certainly imposed a limitation to any conclusion on the role of reflection in ENSO variability, especially during the 90's when observed warmings showed a **behaviour** different from the **El Niño** events in the 80's. There is no doubt that longer time series of **altimetric** data will considerably help in detecting the different processes and understanding the mechanisms responsible for the **interannual** climate variability in the tropical Pacific.

Acknowledgements.

The research described in this paper was carried out by the Jet Propulsion Laboratory, California Institute of Technology, under contract with National Aeronautics and Space Administration. The authors want to thank the "Département d'Océanographie Spatiale de l'IFREMER" for the provision of the ERS-1 scatterometer data. The authors are grateful to Claire Perigaud for her fruitful comments, to Greg Pihos and Akiko Hayashi for their assistance with processing the TOPEX/POSEIDON data and to Nicolas Grima for his help in retrieving the ERS-1 data. Fruitful comments by Nathan Mantua and an anonymous reviewer helped the authors to improve this work. Support from the TOPEX/POSEIDON Project and the NSCAT Project is acknowledged.

REFERENCES

- Battisti D. S., Dynamics and thermodynamics of a warming event in a coupled tropical atmosphere-ocean model, *J. Atmos. Sci.*, 45, 2889-2819, 1988.
- Boulangier, J.-P, and C. Menkes, Propagation and reflection of long equatorial waves in the Pacific ocean during the 1992-1993 El Niño, *J. Geophys. Res.*, **100**, 25041-25059, 1995.
- Callahan, P. S., TOPEX/POSEIDON Project GDR Users Handbook, JPL D-8944 (internal document), rev. A, Jet Propulsion Laboratory, Pasadena, Calif., 84pp, 1994.
- Delcroix, T., J. Picaut, and G. Eldin, Equatorial Kelvin and Rossby waves evidenced in the Pacific Ocean through GEOSAT sea level and surface current anomalies, *J. Geophys. Res.*, 96 suppl., 3249-3262, 1991.
- Delcroix, T., J.-P. Boulangier, F. Masia, and C. Menkes, GEOSAT-derived sea level and surface-current anomalies in the equatorial Pacific, during the 1986-1989 El Niño and La Niña, *J. Geophys. Res.*, 99, 25093-25107, 1994.
- duPenhoat, Y., T. Delcroix and J. Picaut, Interpretation of Kelvin/Rossby waves in the equatorial Pacific from model-GEOSAT data intercomparison during the 1986-1987 El Niño, *Oceanol. Acts*, 15, 545-554, 1992.
- Fu, L.-L., E. J. Christensen, C. Yamarone, M. Lefebvre, Y. Menard, M. Dorrer, and P. Escudier, TOPEX/POSEIDON mission overview, *J. Geophys. Res.*, 99, 24369-24381.
- Hayes, S. P., I., J. Mangum, J. Picaut, A. Sumi, and K. Takeuchi: TOGA-TAO: A moored array for real-time measurements in the tropical Pacific ocean, *Bull. Am. Met. Soc.*, 72, 3, 339-347
- Kessler, W. S., and M. J. McPhaden, Oceanic equatorial waves and the 1991-1993 El Niño, *J. Climate*, 8, 1757-1774, 1995.
- Kessler, W. S., and J. P. McCreary, The annual wind-driven Rossby wave in the subthermocline equatorial Pacific, *J. Phys. Oceanogr.*, 23, 1192-1207, 1993.
- Ii, B., and A. J. Clarke, An examination of some ENSO mechanisms using the interannual sea level at the eastern and western equatorial boundaries and the zonal averaged equatorial wind, *J. Phys. Oceanogr.*, 24, 681-690, 1994.

- Ma, X. C., C. K. Shum, R. J. Eanes, and B. D. Tapley, Determination of ocean tides from the first year of TOPEX/POSEIDON altimeter measurements, *J. Geophys. Res.*, 99, 24809-24820, 1994.
- Mantua, N. J. and D. S. Battisti, Evidence for the delayed oscillator mechanism for ENSO: The "observed" oceanic Kelvin mode in the far western Pacific, *J. Phys. Oceanogr.*, 24, 691-699, 1994.
- McPhaden M. J., TOGA-TAO and the 1991-93 El Niño-Southern Oscillation event, *Oceanography*, 6,36-44, 1993.
- Menkes, C., J.-P. Boulanger, and A. J. Busalacchi, Evaluation of TOPEX/POSEIDON sea level and basin-wide TOGA-TAO sea-surface topographies and derived geostrophic currents, *J. Geophys. Res.*, December 1995.
- Picaut, J., and T. Delcroix, Equatorial wave sequence associated with warm pool displacements during the 1986-1989 El Niño-La Niña, *J. Geophys. Res.*, 100, 18393-18408, 1995.
- Picaut, J., C. Menkes, J.-P. Boulanger, and Y. duPenhoat, Dissipation in a Pacific equatorial long wave model, TOGA-Notes, 10, Nova Univ. Press, Dania, FL, 11-15, 1993.
- Ray, R. D., B. V. Sanchez, and D. E. Cartwright, Some extensions to the response method of tidal analysis applied to TOPEX/POSEIDON altimetry, *EOS Trans. AGU*, 75 (16), Spring meeting Suppl., 108, 1994.
- Schopf, P. S., and M. J. Suarez, Vacillations in a coupled ocean-atmosphere model, *J. Atmos. Sci.*, 45,549-566, 1988.
- Smith, S. D., Coefficients for sea surface wind stress, heat flux, and wind profiles as a function of wind speed and temperature. *J. Geophys. Res.*, 93, 15467-15472, 1988.
- Wyrtki, K., El Niño: the dynamic response of the equatorial Pacific to atmospheric forcing, *J. Phys. Oceanogr.*, 14,242-254, 1984.

FIGURE CAPTIONS

Figure 1: Meridional structures of sea level for Kelvin and first Rossby modes (calculated for a 2.5 m/s Kelvin phase speed). Wave amplitude at a given latitude can be obtained by multiplying the meridional structure to the calculated wave coefficient, yielding in cm.

Figure 2a-d: (a) Standard deviation of TOPEX/POSEIDON sea level anomalies (contour interval is 1 cm); (b) Standard deviation of reconstructed sea level anomalies from Kelvin and first Rossby wave contributions (contour interval is 1 cm); (c) map of correlation between TOPEX/POSEIDON sea level anomalies and sea level reconstructed from Kelvin and first Rossby wave contributions (contour intervals are 0.1 from 0. to 0.9, and 0.04 from 0.90 to 0.98); (d) Map of the variance of TOPEX/POSEIDON sea level anomalies explained by the Kelvin and first Rossby waves (contour intervals are 10% from 10% to 90%, and 4% from 90% to 98%).

Figure 3: Longitude-time plots of (a: left) TOPEX/POSEIDON Kelvin coefficient; (b: right) simulated wind-forced Kelvin coefficient. Coefficients are non-dimensionnalised (contour interval is 10 units). A coefficient of 10 units corresponds to a sea level amplitude of 3.2 cm at the equator for the Kelvin wave.

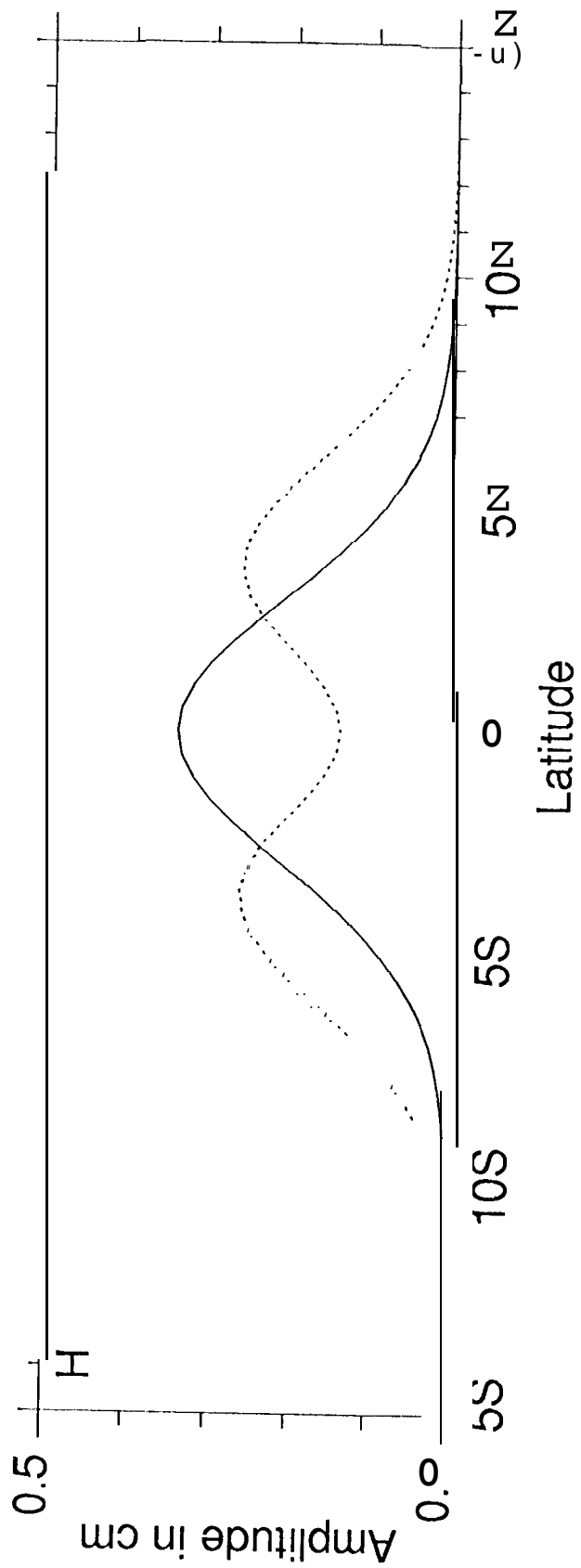
Figure 4: Longitude-time plots of (a: left) TOPEX/POSEIDON first-mode Rossby wave coefficient; (b: right) simulated wind-forced first-mode Rossby wave coefficient. Coefficients are non-dimensionnalised (contour interval is 10 units). A coefficient of 10 units corresponds to a sea level amplitude of 2.8 cm at 4°N for the first-mode Rossby wave.

Figure 5: Longitude-time plots of the TOPEX/POSEIDON Kelvin wave coefficient (from 130°E to 80°W), the first-mode Rossby wave coefficient (in reverse display from 80°W to 130°E) and the Kelvin wave coefficient (from 130°E to 80°W; repeated for comparison). Contour interval is 10 units for both coefficients.

Figure 6: (a: top left) Time series at 84°W of the Kelvin coefficient lagged by a 10-day period (dotted line) and the first-mode Rossby coefficient (solid line); (b: top right) Same as (a) but at 93°W, with the Kelvin coefficient lagged by a 30-day period; (c: bottom left) Kelvin coefficient time series at 84°W (solid line) and 93°W (dotted line); (d: bottom right) Same as (c) but for the first-mode Rossby wave coefficient.

Figure 7: (a: top) Time series at 144°E of the Kelvin coefficient (solid line), the first-mode Rossby coefficient lagged by a 30-day period (dotted line) and of the difference between the Kelvin coefficient and the Rossby coefficient multiplied by 0.41 (dash-and-dot line); (b: bottom) Time series at 144°E of the simulated wind-forced Kelvin coefficient (dotted line) and of the difference between the Kelvin coefficient and the Rossby coefficient multiplied by 0.41 (solid line)

Figure 8: (a: left) Equatorial section of a longitude-time plot of sea surface temperature (contour interval is 0.5°C); (b: center) Same as (a) but for sea surface temperature anomalies (anomalies arc related to the January 1993 -December 1994 two-year mean; contour interval is 0.5°C); (c: right) Same as (a) but for ERS-1 zonal wind stress anomalies (anomalies are related to the January 1993 -December 1994 two-year mean; contour interval is 0.01Pa).



1.0

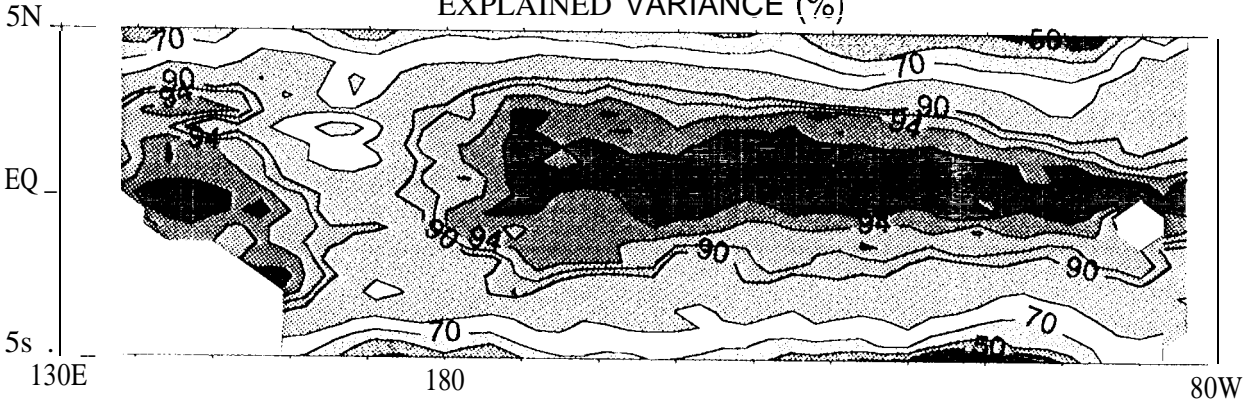
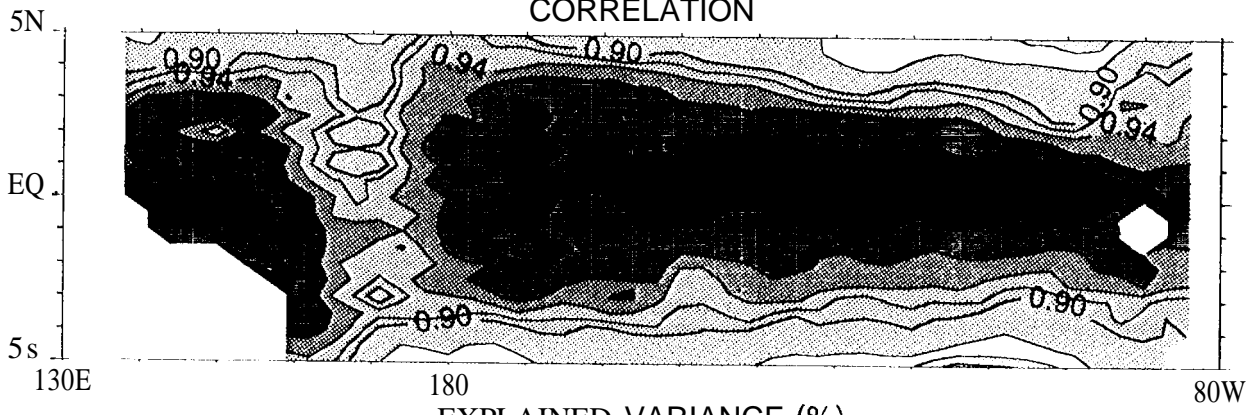
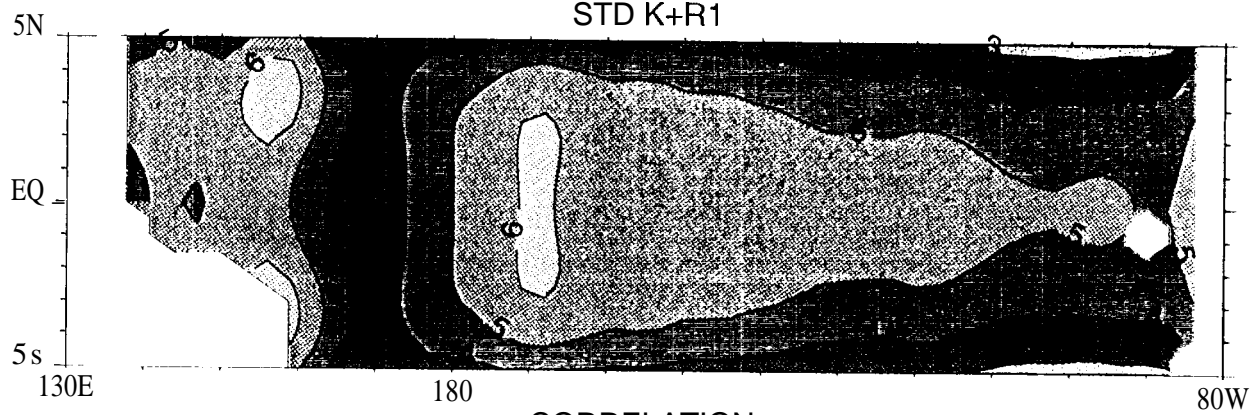
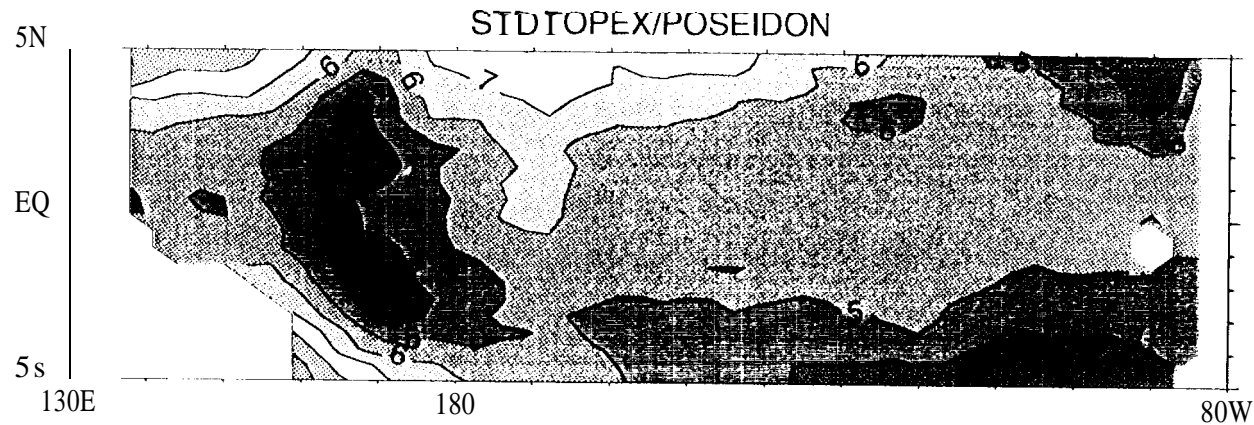


Fig. 2

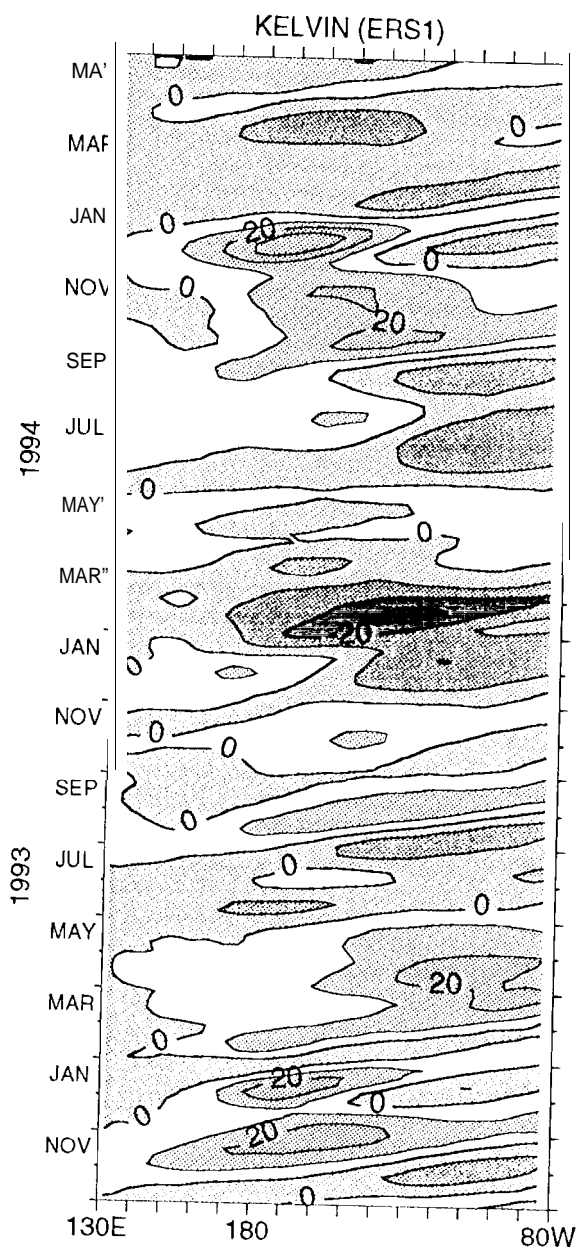
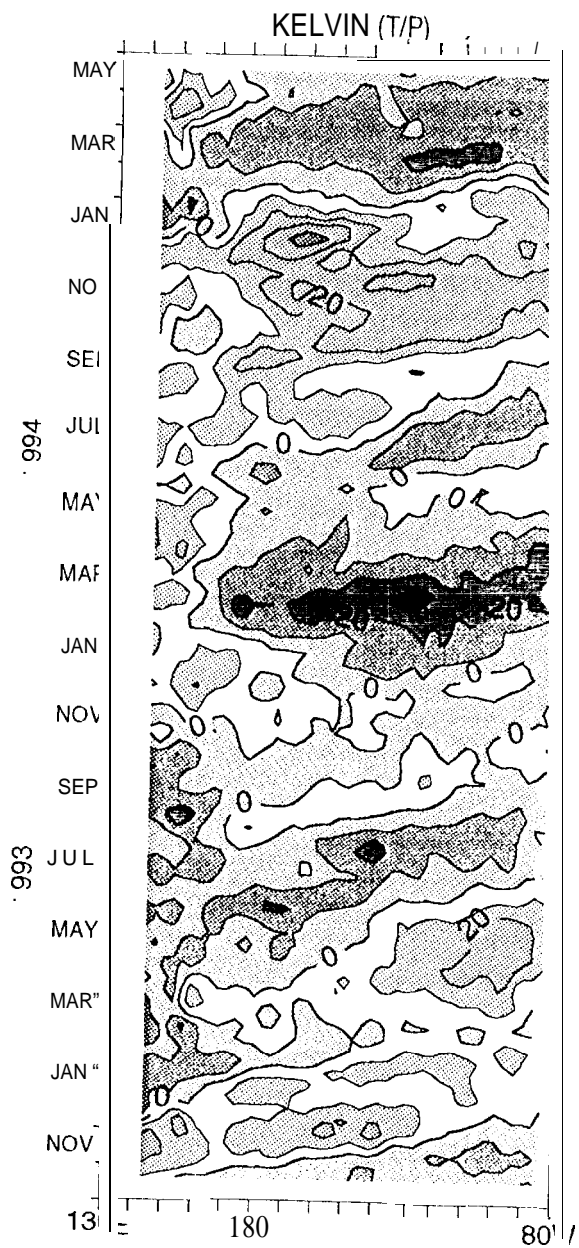
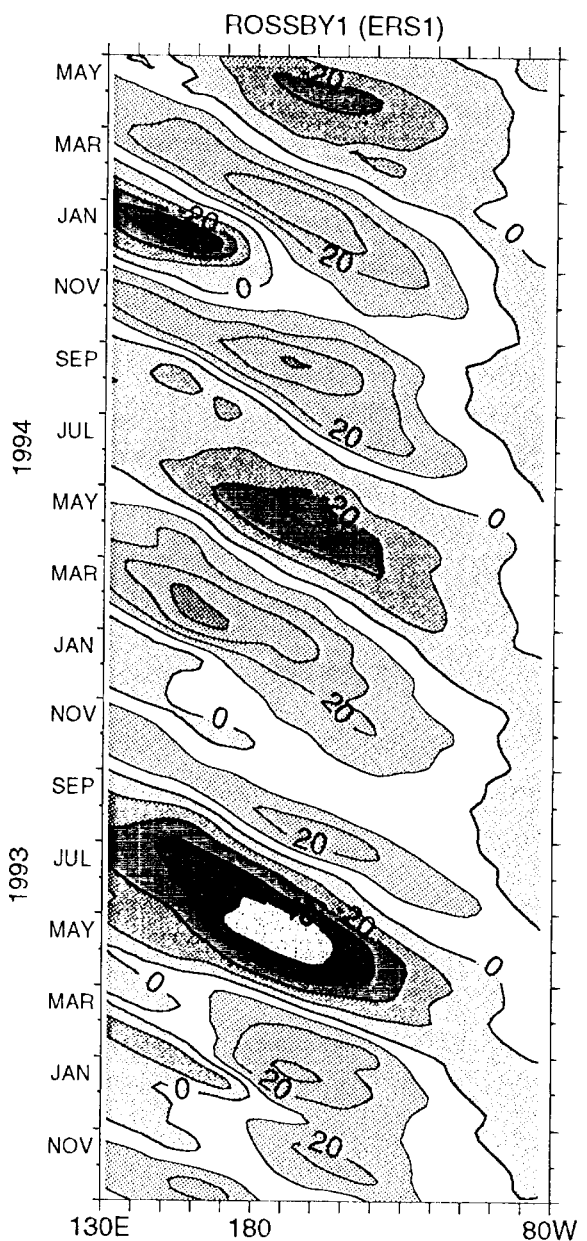
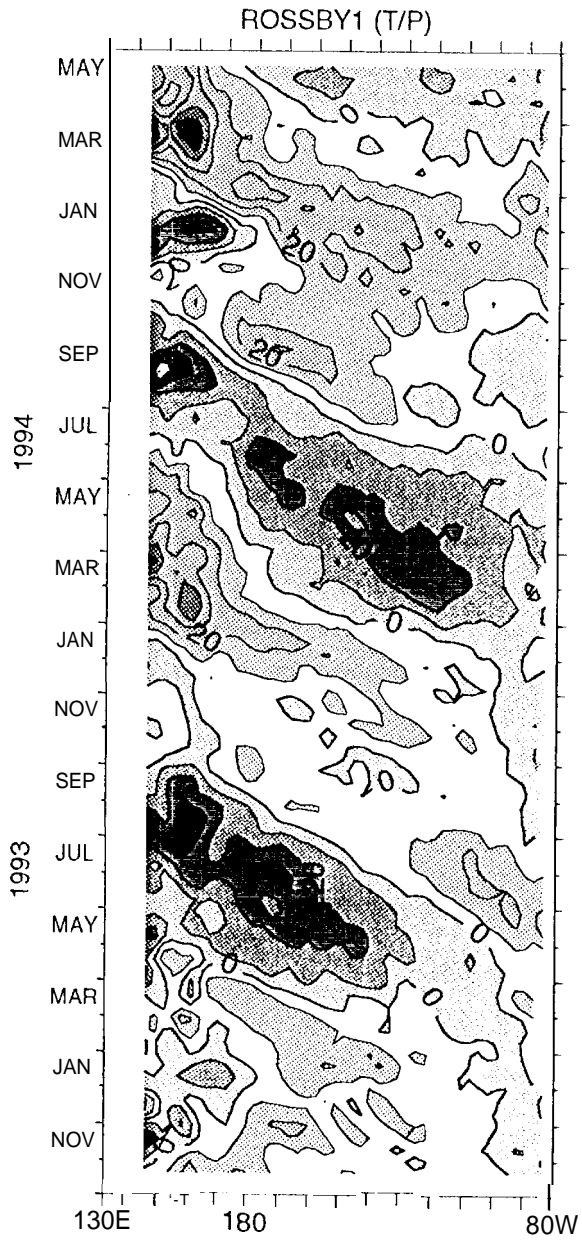
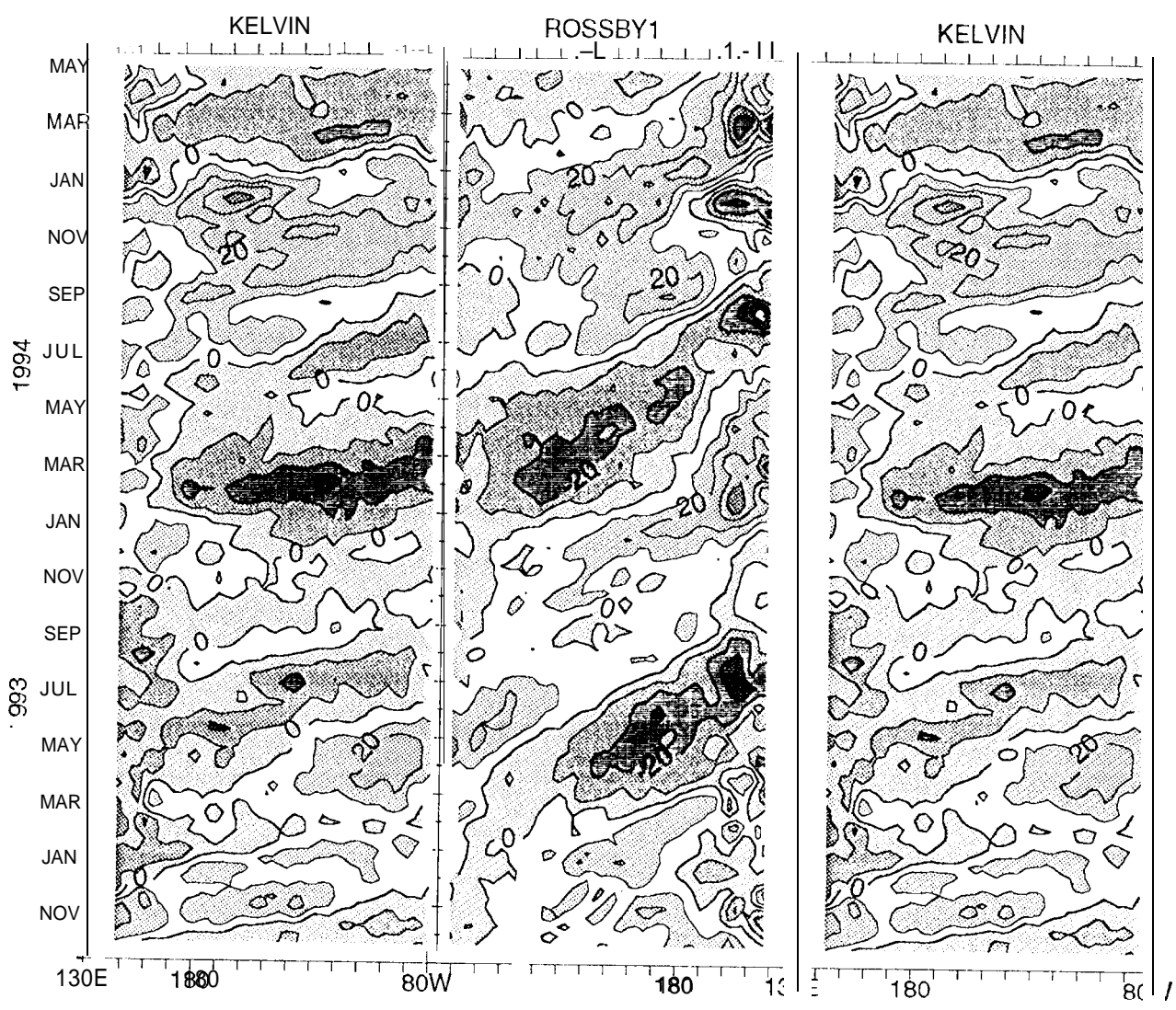
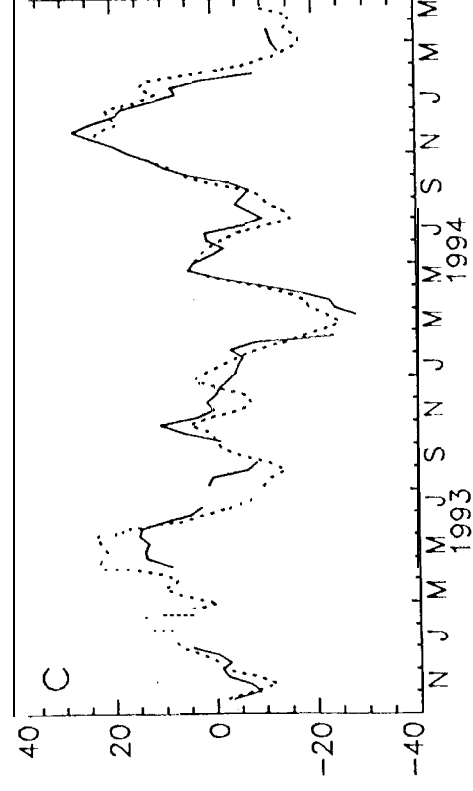
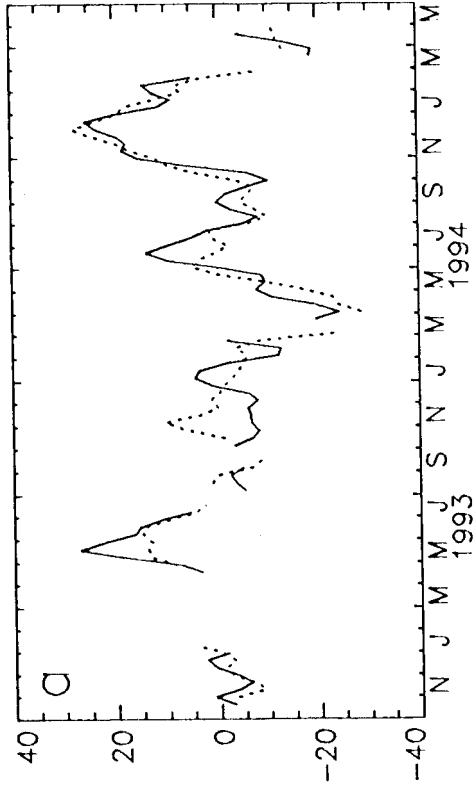
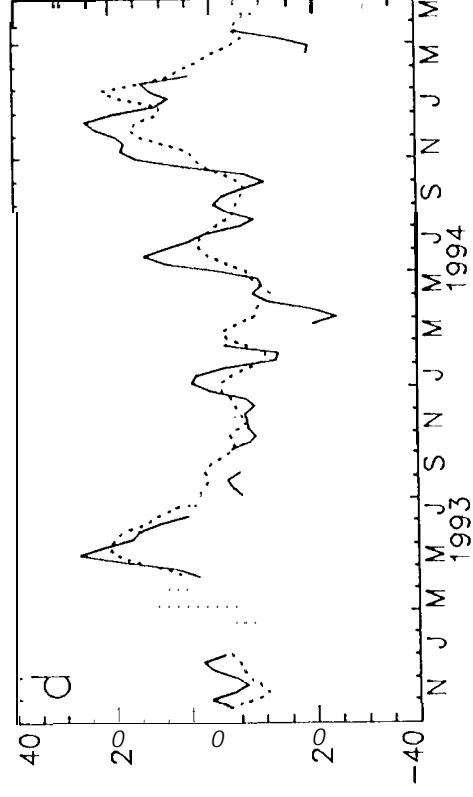
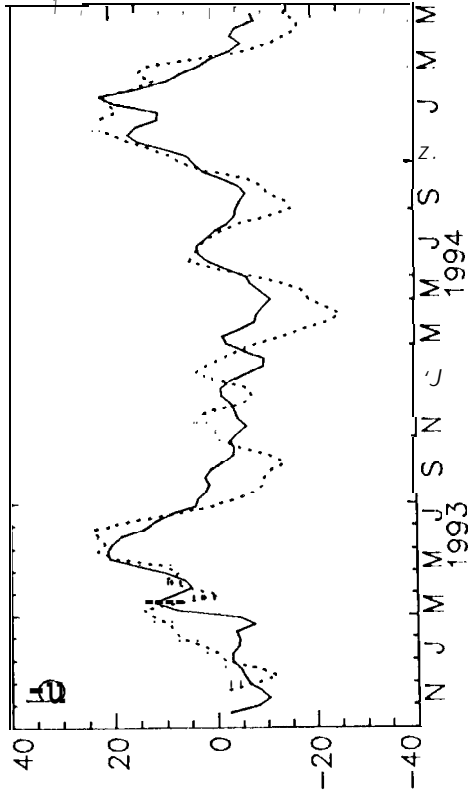


Fig. 3







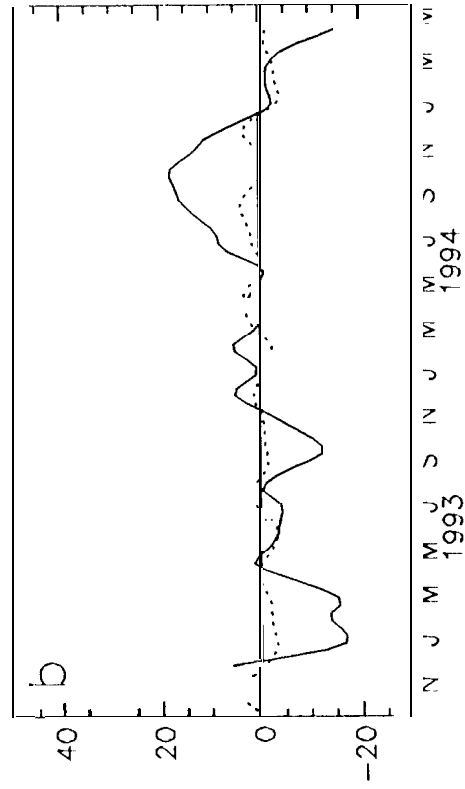
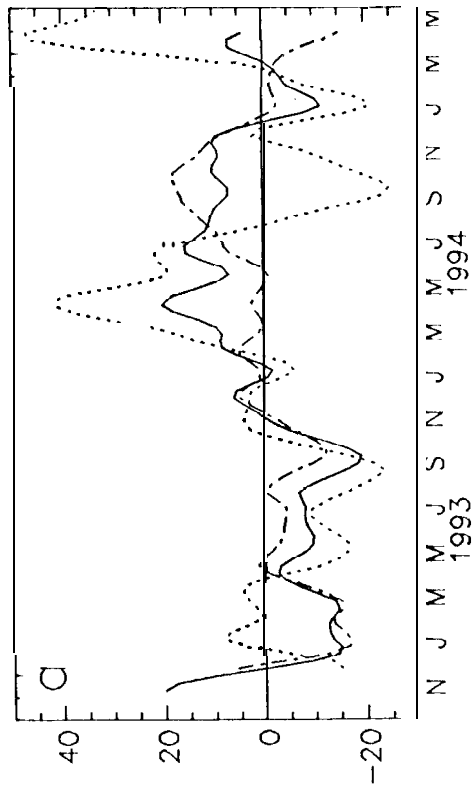


Fig. 7

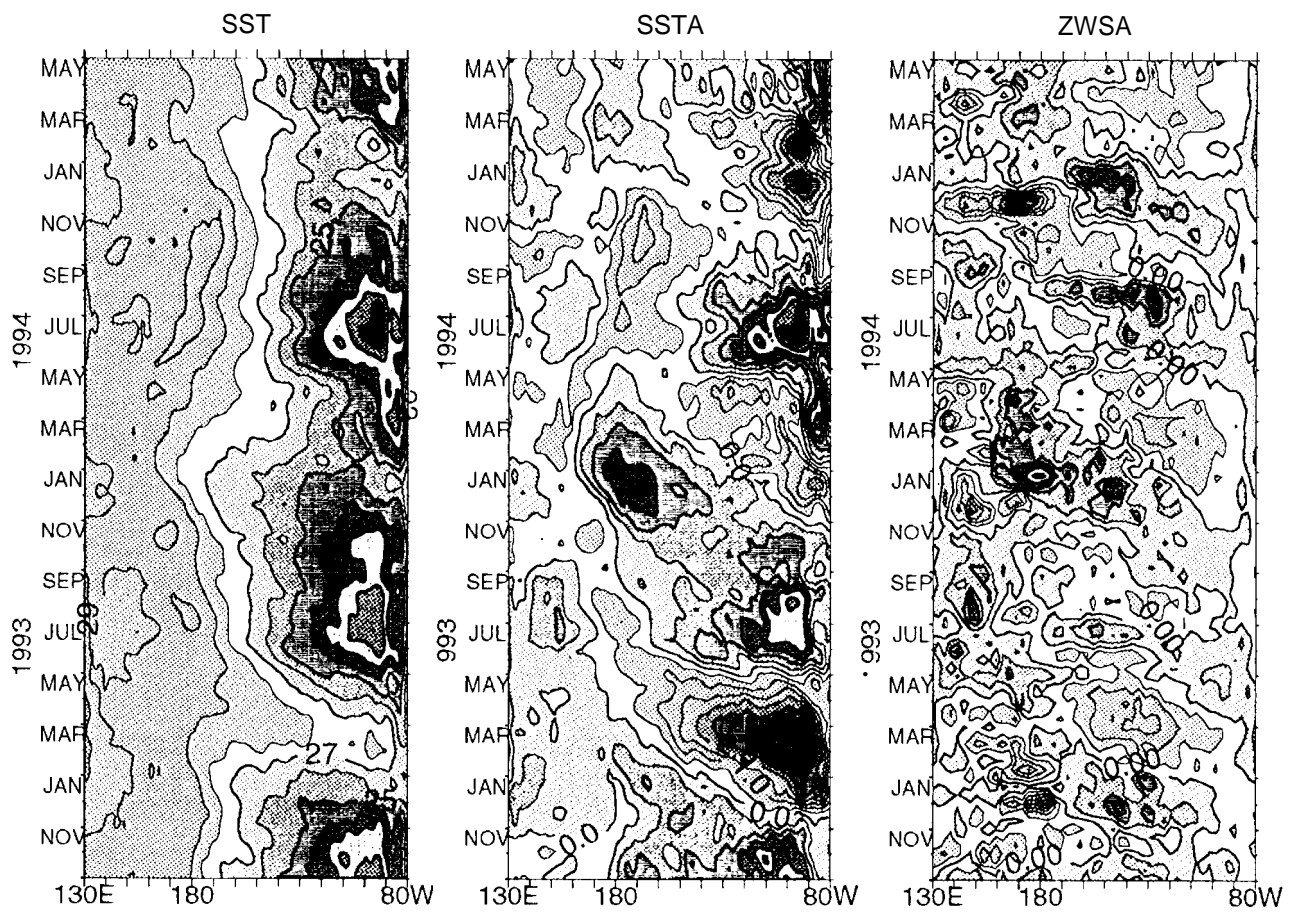


Fig. 7